Journal of Sciences, Islamic Republic of Iran 32(3): 221 - 233 (2021) http://jsciences.ut.ac.ir
University of Tehran, ISSN 1016-1104

Mineral Chemistry and Whole-rock Geochemistry of Pillow lava from the Arangue Complex, Southeastern Hormozgan, Iran

E. Nazari Zadeh, M. Poosti*, A. Nazarinia

Department of Geology, Faculty of Sciences, University of Hormozgan, Hormozgan, Iran, Islamic Republic of Iran

Received: 2 November 2020 / Revised: 11 March 2021 / Accepted: 14 April 2021

Abstract

The Upper Cretaceous Arangue complex is located in the Makran zone at the SE of Iran. The complex consists of ultra-mafic rocks, microgabbro dykes, pillow lavas and lime stones that pillow lavas are mainly exposed to the northwest and southeast part of study area. There are oval and tubular basalt lavas with cracked bread crust surface. They predominantly have plagioclase, clinopyroxene with minor olivine and opaque minerals in a fine-grained groundmass along with glass. Mineral chemistry data show that plagioclases and clinopyroxene composition varies from $An_{68.27-81.73}Ab_{18.27-31.57}Or_{0-0.41}$ and $Wo_{38.1-47.8}Fs_{8.2-19.3}En_{38.6-48.7}$ respectively. In the geochemical diagrams, the Arangue complex pillow lavas fall in the basalt and sub-alkaline fields. Geochemical data indicate that the Arangue complex pillow lavas are tholeiitic. The absence of a distinct Eu anomaly (Eu/Eu*= 0.8-1.2), indicates that plagioclase fractionation is not notable, or that the magma is a little oxidized. The Arangue complex pillow lavas show properties similar to transitional basalts between enriched MORB and OIB and some BABB. However, their enrichment in incompatible elements and low Nb and La / Nb ratios (0.8-2.1) display that these have affinity of the BABB. These were produced by approximately 15-25% partial melting of plagioclase lherzolite where fractionation was controlled by removal of clinopyroxene, spinel, and olivine. Petrogenetic study indicates that the source of mantle lherzolite is subjected to enrichment variables in subduction components consisting of fluids for the Arangue Complex pillow lavas.

Key words: Arangue complex; Pillow lava; MORB; Hormozgan province; Makran.

Introduction

Ophiolites are segments of the upper part of the mantle and ancient oceanic crust emplaced on continental rims and it was created when the continent collided and the ocean closed between them. [1]. The continental of rifting, forming an oceanic crust, over Iran and other Cimmerian blocks like Turkey and Afghanistan, Karakoram was Late Paleozoic-Early Mesozoic time [2].

Iranian ophiolites are a section of the Tethyan ophiolitic belts that ophiolites of the Eastern

* Corresponding author: Tel: 00989164296735; Fax: 00987633711078; Email: m.poosti@yahoo.com

Mediterranean (Hellenides-Dinarides) and Asia are connected [3]. Based on their abundances and age, ophiolites in Iran can be ordered into three main groups: Late Neoproterozoic, the Paleozoic (less abundant), and Mesozoic ophiolites (more abundant) [4]. The oldest areas of Iran in the Central Iran Block contain small outcrops of ophiolite assemblages that Indicates the emergence, expansion, and then closure and destruction of small Late Neoproterozoic oceanic basins on the northern edge of Gondwana (Proto-Tethys) between 800 and 530 million years ago. These collections have been reported in areas such as Misho in the northwest of Tabriz [5], Jandagh-Arousan [6, 7], Saghand-Posht-e-Badam [8], Takab [9, 10] and Khoy [11, 12,13].

However, geographically they have been classified into four groups [14]: (i) ophiolites located in North of Iran, (ii) ophiolites of Zagros, containing the Neyriz and Kermanshah ophiolites, which seem to be an extension of the Samail (Oman) ophiolite obducted onto the Arabian platform; (iii) ophiolites of the Makran or Jazmurian, which contains the complex of Band-e-Zeyarat/ Dar-e- Anar, Ganj, Rameshk/ Mokhtarabad; (iv) ophiolitic coloured mélange complexes such as Shahr-e- Babak and Tchehel Kureh ophiolites that detect the boundaries of the Central Iranian Microcontinent (Fig. 1).

Also, according to further studies [eg 2 17] ophiolite in Iran contains Zagros in the southwest, Makran in the southeast, Khoy in the northwest, Sabzevar in the northeast and Birjand-Nehbandan in the east (Fig. 1). The so-called Arangue complex belong to Makran ophiolites [18].

Previous studied have been suggested for the magmatic evolution and geodynamic setting of the Makran ophiolites. McCall and Kidd [19] studied Makran coloured mélange and proposed that they were produced during scratching oceanic plate on the Makran, whereas the Makran ophiolite (inner) was generated in a back-arc environment. Based on the geochemical natures of lavas, a mid-oceanic ridge setting proposed for the Makran ophiolites (inner) including the Band-e- Zeyarat, [20]. Moslempour et al.,

Figure 1. Simplified map of Iran and the position of Makran areas. Distribution of the ophiolites among the Eurasian and Arabian plates [15, 16].

[21, 22] suggested the model of the SSZ (Sanandaj Sirjan Zone) back-arc basin for the organization of the Makran ophiolite (inner) [23]. Furthermore, Shahabpour [24] believe that the Makran ophiolites was formed in an extensional environment. The volcanic rocks in the outer Makran ophiolites have been identified by various geochemical natures [25].

The aim of this study, are 1) presentation of field, petrography, mineral and whole rock chemistry of the pillow lavas for the first time and 2) using these data in order to clarifying petrological evolutions of pillow lavas from the Arangue complex.

Geological background

The Makran zone is an accretionary prism made upper subduction zone, during subducting Indian Ocean crust under the Lut continental block [26]. The Makran have 450 km in length, from southeastern Iran to southwestern Pakistan and contains an area about 200 km wide between the Jazmurian belt and sea of Oman [26].

Iranian Makran zone could be divided into six zones [19, 27], including the Cenozoic Makran magmatic arc, the Jazmurian belt, the Makran ophiolites (Inner and outer), the Bajgan/Durkan complex and the Makran flysh zone. Except for the areas pointed above, the Arangue colored mélange complex is less noticed. The Upper Cretaceous Arangue colored mélange complex is located in the Makran structural zone at the SE of Iran [18]. This complex (Trending NW-SE) consists of ultramafic rocks, micro gabbro dykes, pillow lavas and limestones (Fig. 2); [18]. Pillow lavas are generally

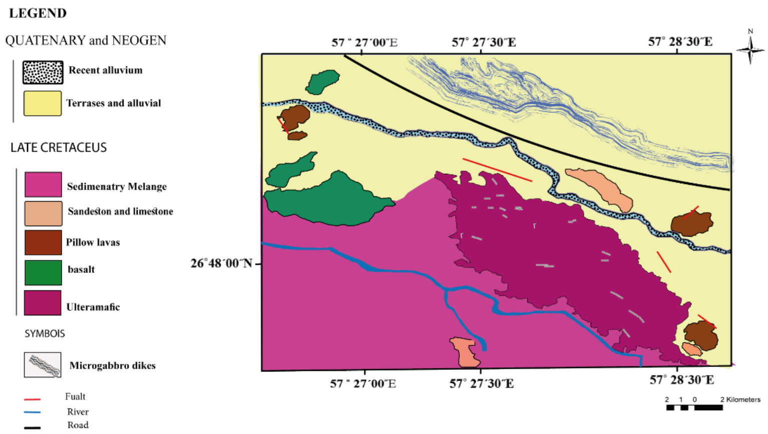

Figure 2. Simplified geological map of the study area (Arangue complex), southeast of Hormozgan

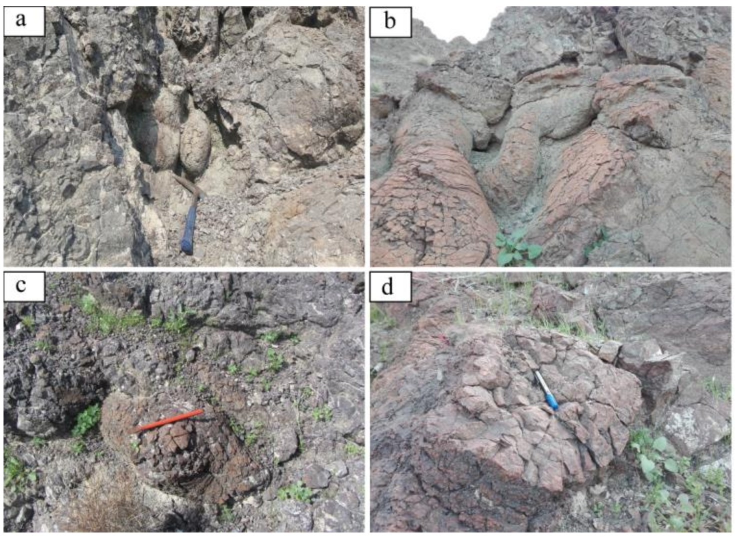

Figure 3. Field photographic showing different morphology of the pillow lava outcrops at Arangue complex. (a) Oval shape. (b) Tubular shape. (c) Bread crust crack surfaces. (d) Cross section of pillow showing radial fractures.

exposed to the northwest and southeast part of the study area (Fig. 2). Their shape are commonly oval and tubby. Its diameter is from 0.2 to 3 meters (Fig. 3a-b).

According to classification of pillow lava [28], the Arangue complex pillow lavas can be divided to normal and mega pillows with <100 cm and > 1 to 3 meters in length respectively. They have different shapes and features, mostly oval and tubular with bread crust crack surface (Fig. 3c). These are associated with their growth mechanism. Monotonous stretching of the outer crust mainly creates small pillows with smooth-surface and unbroken chilled crusts [28, 29]. Slower extrusion rates favor regular spreading with subsequent spreading and development of ruptures on chilled crust surfaces; as observed in the Arangue complex pillow lavas.

They have a series of radial fractures converge towards the center (Fig. 3d) that many of these fractures are now filled with secondary mineral such as calcite and chlorite.

Materials and Methods

The petrographic studies were done over 40 thin sections of pillow lavas from the Arangue complex were prepared for petrographic study. Microprobe analysis of minerals such as plagioclase and clinopyroxene was performed at the Iranian Mineral Processing Research Center (IMPRC) in Karaj (Tables 1 and 2). The Cameca SX-100 microprobe worked with a voltage of 20 kv, a beam current of 25 nA and a mixture size of 3 micrometers. Ten (10) samples were analysed by X-ray fluorescence (XRF) and ICP-MS in geochemistry laboratory of the Geological Survey and Mineral Exploration in Tehran- Iran (Table 3). 100 mg of each sample is putted in sealed polyethylene bags and irradiate the γ-ray spectrum for 1 hour with a thermal neutron flux of about 2.8×1013 n cm_1 s_1 and were 100 measured after cooling for about 1 and 3 weeks: The counting time was 1.5 hours for the first and 3 hours for the second.

Results

Petrography

The Pillow lavas of Arangue complex were particulary obtained from the volcano-sedimentary

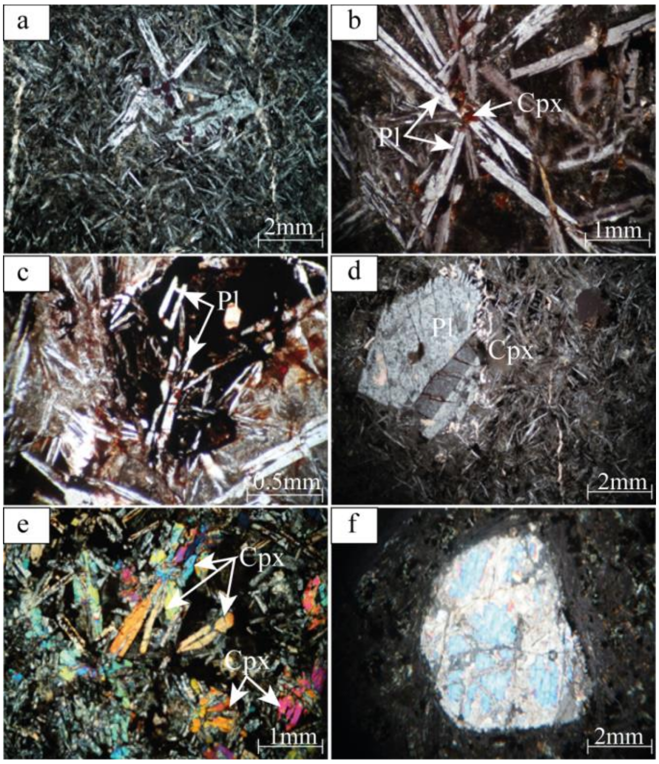

Figure 4. Crossed polorized light representative photomicrographs of the Arangue complex. (a) Microlitic and glomeroporphyritic texture. (b) Plagioclase microlite and clinopyroxene with a variety of spherulitic forms in a groundmass. (c) Hollow plagioclase microlites in the pillow lava. (d) Plagioclase dendrites. (e) Euhedral to subhedral clinopyroxene in the samples. (f) Vesicle filled with secondary minerals. Mineral abbreviations based on [30]: Pl, plagioclase; Cpx, clinopyroxene.

sequence. Samples are basalt in composition. They commonly have plagioclase (70-80 vol. %), clinopyroxene (10-20 vol. %) with minor olivine and opaque minerals in a fine-grained groundmass along with glass. They show microlitic, porphyritic, intersertal, vesicular and glomeroporphyritic textures (Fig. 4a). Plagioclase occurs as euhedral to subhedral elongated phenocrysts (> 3mm in size) and microlitic lath, with a variety of spherulitic forms in a groundmass (Fig. 4b). Plagioclase phenocrysts commonly show albite-carlsbad twining. Also, hollow plagioclase microlites are observed (Fig. 4c). Commonly dendritic fibers or arms are observed at the plagioclase terminations (Fig. 4d). Plagioclase phenocrysts and microlites are rarely show sericitization and carbonitization.

Table 1. Representative electron microprobe analyses (in wt%) of plagioclases from the Arangue complex. Pl=Plagioclase

Sample	**A412-22**	**A412-23**	**A412-24**	**A412-25**	**A412-26**	**A412-27**	**A412-28**
Mineral	Pl	Pl	Pl	Pl	Pl	Pl	Pl
SiO_2	46.96	49.11	48.20	49.21	46.49	47.61	46.12
TiO_2	0.01	0.02	0.01	0.03	0.01	0.02	0.01
Al_2O_3	30.30	28.36	29.34	30.31	31.30	28.94	30.34
FeO	0.14	0.25	0.15	0.13	0.14	0.15	0.14
MnO	bd	bd	bd	bd	bd	bd	bd
MgO	bd	bd	bd	bd	bd	bd	bd
CaO	18.98	17.24	18.34	17.16	18.99	19.00	18.32
Na_2O	3.24	3.80	2.90	3.03	3.22	3.20	3.24
K_2O	0.00	0.02	0.05	0.00	0.00	0.05	0.00
Total	99.63	98.80	98.99	99.87	100.15	98.97	98.17
Structural formula							
Si	1.89	1.99	1.95	1.97	1.86	1.92	1.88
Ti	nc	nc	nc	nc	nc	nc	nc
Al	1.62	1.53	1.58	1.62	1.67	1.56	1.65
Fe	0.01	0.02	0.01	0.01	0.01	0.01	0.01
Mn	nc	nc	nc	nc	nc	nc	nc
Mg	nc	nc	nc	nc	nc	nc	nc
Ca	1.52	1.40	1.48	1.37	1.52	1.54	1.49
Na	0.52	0.62	0.47	0.49	0.51	0.52	0.53
K	0.00	0.00	0.01	0.00	0.00	0.01	0.00
Total	5.56	5.55	5.50	5.46	5.57	5.56	5.56
Or	0.00	0.16	0.41	0.00	0.00	0.39	0.00
Ab	25.45	30.55	23.93	26.10	25.32	25.10	26.13
An	74.55	69.29	75.66	73.90	74.68	74.51	73.87

Sample	**A14-3**	**A14-4**	**A14-5**	**A14-9**	**A14-10**	**A14-11**	**A13-15**
Mineral	Pl	Pl	Pl	Pl	Pl	Pl	Pl
SiO_2	49.32	46.86	49.24	48.32	49.25	49.11	49.12
TiO_2	0.01	0.02	0.02	0.01	0.03	0.02	0.01
Al_2O_3	28.39	31.30	28.47	29.45	30.67	28.46	28.45
FeO	0.15	0.14	0.15	0.16	0.14	0.23	0.22
MnO	bd	bd	bd	bd	bd	bd	bd
MgO	bd	bd	bd	bd	bd	bd	bd
CaO	18.94	17.98	18.24	18.54	18.16	17.34	17.31
Na_2O	3.33	3.24	3.18	3.20	2.03	4.01	3.99
K_2O	0.00	0.00	0.02	0.05	0.00	0.02	0.01
Total	100.14	99.54	99.32	99.73	100.28	99.19	99.11
Structural formula							
Si	1.97	1.88	1.98	1.94	1.96	1.98	1.98
Ti	nc	nc	nc	nc	nc	nc	nc
Al	1.51	1.68	1.53	1.57	1.63	1.53	1.53
Fe	0.01	0.01	0.01	0.01	0.01	0.02	0.02
Mn	nc	nc	nc	nc	nc	nc	nc
Mg	nc	nc	nc	nc	nc	nc	nc
Ca	1.51	1.44	1.47	1.49	1.45	1.40	1.40
Na	0.53	0.52	0.51	0.51	0.32	0.65	0.64
K	0.00	0.00	0.00	0.01	0.00	0.00	0.00
Total	5.54	5.54	5.51	5.53	5.38	5.58	5.57
Or	0.00	0.00	0.16	0.40	0.00	0.16	0.08
Ab	26.02	26.49	25.81	25.56	18.27	31.57	31.53
An	73.98	73.51	74.03	74.04	81.73	68.27	68.39

The Structural formula of plagioclase was calculated based on 8 oxygens.bd: below detection limit; nc: not calculated.

Euhedral to subhedral clinopyroxene (Fig. 4e) (<0.1 mm in size) is often replaced by uralite and chlorite. Clinopyroxenes create glomeroporphyric texture and poikilitically enclose plagioclase and opaque minerals.

Olivines are an infrequent and observe only in some samples as fine phenocrysts, generally replaced by iddingsite.

Opaque minerals occur as acicular and dendritic crystals in the groundmass. In addition, they are produced on the rims of the clinopyroxene microphenocryst. It is produced by the alteration of secondary minerals such as calcite, chlorite, epidote, zeolite, quartz and iron oxides. Vesicles and amygdules filled with zeolite, calcite, chlorite and/or quartz are prevalent in the pillow lava from the Arangue complex (Fig. 4d).

Mineral chemistry

The chemical composition of the major element of plagioclase and clinopyroxene from the Arangue complex are listed in Table 1 and 2. They have a compositional range of $An_{68.27}$ to $An_{81.73}$ and occur primarily as bytownite and Labradorite in composition (Table 1, Fig. 5a).

Clinopyroxenes from pillow lava have compositions ranging from augite to diopside ($Wo_{38.1}Fs_{8.2}En_{38.6}$ to $Wo_{47.8}Fs_{19.3}En_{48.7}$; see Table 2). They have Mg number (Mg#) ranging from 66.4 to 84.8 (Fig. 5b).

Whole-rock Geochemistry

All the Arangue complex pillow lava are approximately affected by submarine hydrothermal that it is a nature of other ophiolite basalts [33, 34].

Studies of chemical changes due to alteration have revealed mobilities of most major oxides and large ion lithophile elements (called LILE, such as Ba and Rb). These elements are unlikely to show primary composition [35]. Thus, selected elements such as zirconium (Zr), Niobium (Nb), Titanium (Ti), Yttrium (Y), Tantalum (Ta) and rare earth elements (REEs), may be used to characterize altered basic volcanics according to their petrological natures and tectonic setting [36, 37, 38, 39].

In the Figures 6a and 6b [40], the Arangue complex fall in the basalt and sub-alkaline fields respectively. Moreover, the low ratios of Zr/Y (4.7-6.8), La/Nb (0.8-2.1) and Nb/Y (0.05-0.2) indicate their sub-alkaline (tholeiitic) feature [40] (Table 3).

The Figures 6c and 6d show that the Arangue complex pillow lavas have similarities to MORB and BABB, rather than IAT [41]. The Figure 6d is considered to be the foremost discriminant for tectonic setting and these values are expounded to reflect origin content [41].

Similarity of geochemical pattern of the Arangue complex pillow lavas to MORB, BABB and island arcs would be create using the high ionic potential elements which are considered immobile during alteration [42]. On N-MORB normalized spider diagram (Fig. 7a) the Arangue complex show enrichment in LILE relative to MORB.

The Figure 7b shows light rare earth elements (LREEs) enrichments (Fig. 7b) relative to heavy rare earth elements (HREEs). The absence of a distinct Eu anomaly (Eu/Eu*= 0.8-1.2), indicates that plagioclase fractionation is not notable, or that the magma is a little oxidized.

Discussion

Based on studies by many authors (e.g., [33, 44]) on basalt rocks, the composition of their incompatible elements largely depends on the degree of partial melting of the correlated mantle origin, whereas it is slightly controled by fractional crystallization process (e.g., [44]).

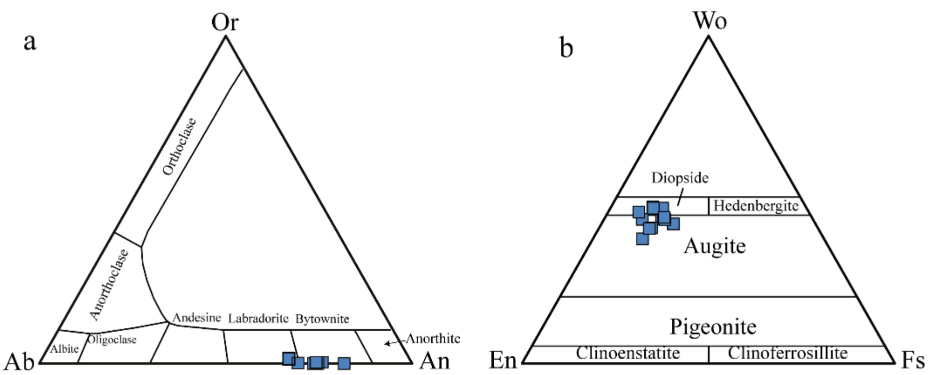

Figure 5. (a) An-Ab-Or triple scheme and position of feldspars on it [31]. (b) Clinopyroxene classification diagram [32].

Table 2. Electron microprobe analyses (in wt%) of pyroxene from the Arangue complex. Px=Pyroxene

Sample	A412-16	A412-17	A412-18	A412-19	A412-20	A412-21	A14-1
Mineral	Px	Px	Px	Px	Px	Px	Px
SiO_2	53.92	50.79	51.29	51.87	51.83	50.52	50.08
TiO_2	0.46	1.21	0.96	0.75	0.99	1.46	1.78
Al_2O_3	1.94	3.31	4.25	1.85	3.1	3.47	4.91
Cr_2O_3	bd	bd	bd	bd	bd	bd	bd
FeO	6.75	10.29	6.68	9.89	6.59	12.11	9.47
MnO	0.18	0.22	0.13	0.31	0.16	0.28	0.19
MgO	17.4	13.63	15.64	15.38	15.73	12.8	13.38
CaO	18.94	20.61	20.88	19.87	22.18	19.89	20.57
Na_2O	0.21	0.38	0.26	0.2	0.26	0.34	0.36
K_2O	bd	bd	bd	bd	bd	bd	bd
Total	99.8	100.44	100.09	100.12	100.84	100.87	100.74
Cation (Structural Formula on the basis of 6 Oxygen)							
Si	1.979	1.889	1.884	1.926	1.892	1.886	1.855
Ti	0.013	0.034	0.027	0.021	0.027	0.041	0.05
Al	0.084	0.145	0.184	0.081	0.133	0.153	0.214
Al_{IV}	0.03	0.10	0.11	0.07	0.10	0.11	0.14
Al_{VI}	0.05	0.04	0.07	0.01	0.03	0.04	0.07
Cr	nc	nc	nc	nc	nc	nc	nc
Fe^{3+}	-0.052	0.036	0.014	0.041	0.047	0.018	0.002
Fe^{2+}	0.259	0.284	0.191	0.266	0.154	0.36	0.292
Mn	0.006	0.007	0.004	0.01	0.005	0.009	0.006
Mg	0.952	0.756	0.856	0.851	0.856	0.712	0.739
Ca	0.745	0.821	0.822	0.79	0.867	0.796	0.817
Na	0.015	0.027	0.019	0.014	0.018	0.025	0.026
K	nc	nc	nc	nc	nc	nc	nc
Total	4	4	4	4	4	4	4
En	48.7	40.6	45.8	44.6	45.6	38.1	40
Fs	13.3	15.3	10.2	14	8.2	19.3	15.8
Wo	38.1	44.1	44	41.4	46.2	42.6	44.2
$Mg.(Mg+Fe^{2})$	78.6	72.7	81.7	76.2	84.8	66.4	71.7

Sample	A14-2	A14-7	A14-8	A14-12	A14-13	A13-22	A13-23.
Mineral	Px	Px	Px	Px	Px	Px	Px
SiO_2	50.31	49.64	49.52	48.62	48.43	48.91	49.65
TiO_2	1.7	1.67	1.56	1.83	1.85	2.11	1.14
Al_2O_3	4.38	6.07	4.79	5.58	4.91	4.54	3.16
Cr_2O_3	bd	bd	bd	bd	bd	bd	bd
FeO	10	7.04	7.7	8.73	8.87	9.24	9.83
MnO	0.24	0.18	0.17	0.16	0.16	0.18	0.23
MgO	13.37	13.6	13.44	12.55	13.29	13	14.99
CaO	20.56	22.05	21.71	21.41	21.35	20.43	18.95
Na_2O	0.32	0.34	0.33	0.37	0.37	0.34	0.25
K_2O	bd	0.01	0.01	bd	bd	bd	0.01
Total	100.88	100.59	99.22	99.25	99.23	98.75	98.2
Cation (Structural Formula on the basis of 6 Oxygen)							
Si	1.865	1.827	1.853	1.828	1.818	1.852	1.877
Ti	0.047	0.046	0.044	0.052	0.052	0.06	0.032
Al	0.191	0.263	0.211	0.247	0.217	0.203	0.141
Al_{IV}	0.13	0.17	0.14	0.17	0.17	0.15	0.11
Al_{VI}	0.06	0.09	0.07	0.08	0.05	0.05	0.03
Cr	nc	nc	nc	nc	nc	nc	nc
Fe^{3+}	0.007	0.014	0.018	0.02	0.07	-0.001	0.059
Fe^{2+}	0.303	0.202	0.223	0.255	0.209	0.294	0.252
Mn	0.008	0.006	0.005	0.005	0.005	0.006	0.007
Mg	0.739	0.746	0.75	0.704	0.744	0.734	0.845
Ca	0.817	0.87	0.871	0.863	0.859	0.829	0.768
Na	0.023	0.024	0.024	0.027	0.027	0.025	0.018
K	nc	nc	nc	nc	nc	nc	nc
Total	4	4	4	4	4	4	4
En	39.7	41	40.7	38.6	41.1	39.5	45.3
Fs	16.3	11.1	12.1	14	11.5	15.8	13.5
Wo	43.9	47.8	47.2	47.4	47.4	44.6	41.2
$Mg.(Mg+Fe^{2})$	70.9	78.7	77.1	73.4	78.1	71.4	77

For determine of petrogenesis of the basalts (oceanic or not), authors (e.g., [45, 46]) used ratios diagram of Th/Yb versus Nb/Yb as factor to focus attention on the crustal contamination and Ti/Yb versus Nb/Yb to show

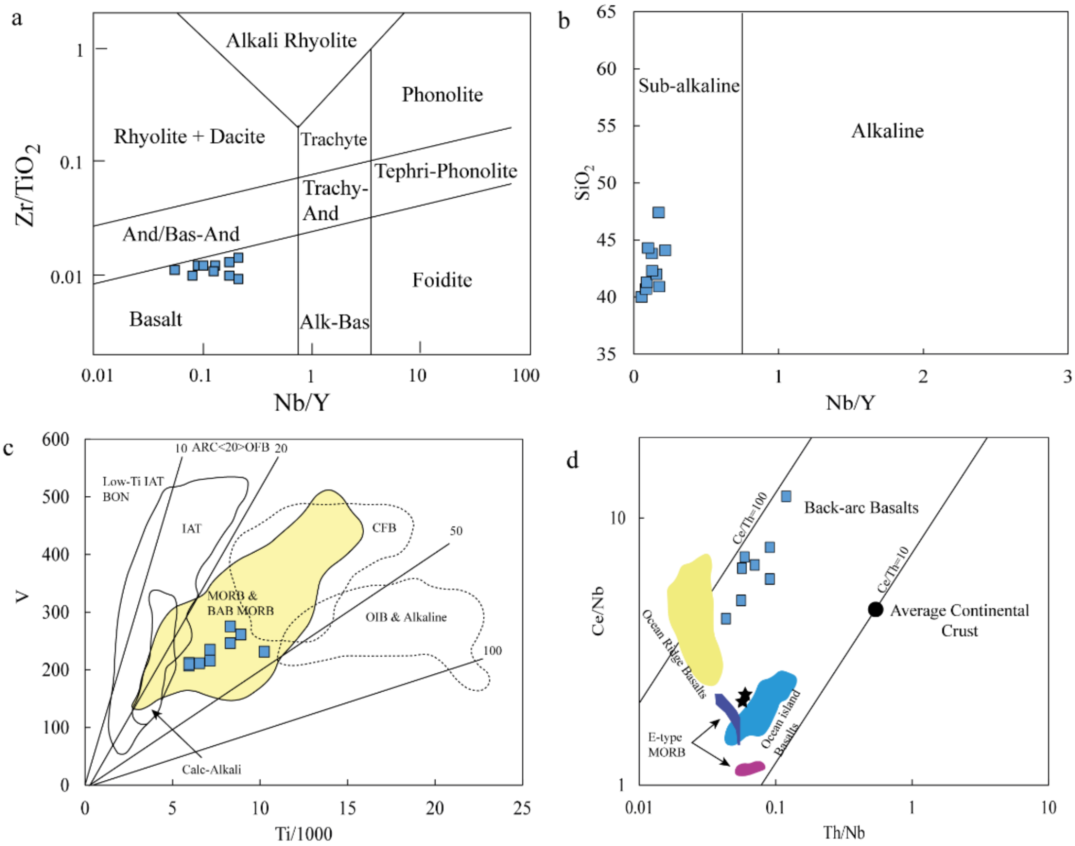

Figure 6. (a) Zr/ TiO_2 versus Nb/Y and (b) SiO_2 versus Nb/ Y diagrams for Arangue complex pillow lavas [40]. (c) Ti versus V diagram [37] (d) Ce/Nb versus Th/Nb diagram for the Arangue complex pillow lavas, fields are from [41]. Symbols are the same as in Table 3.

depth at which the melting took place. Based on the Figure 8a, the Arangue complex pillow lavas show present day MORB with a little evolution towards OIB, and when magma ascends, they react with the continental crust or display a subduction component then they locate over the MORB-OIB line or on a vector at a sloping angle to the line, reflecting selective Th addition [46].

On the Figure 8b, N-MORB and E-MORB affinities are clear. The Arangue complex pillow lavas show their MORB natures with tendency towards both E-MORB and OIB compositions with no sign of crustal involvement, either direct crustal contamination or through hereditary subduction components in the lithosphere (Fig. 8b).

Draw compatible elements versus incompatible elements is a method to estimate the degree of depletion of the mantle. In generally, compatible element abundance has not remarkably changed during the mantle depletion. In contrast the abundance of other elements (e.g incompatible) has closely associated to degree of melting and source depletion [44]. We therefor use Cr versus Y diagram [44, 48] shown in Figure 8c for determining of the sources Arangue Complex pillow lavas. In this diagram, there are two possible sources of mantle: (1) a depleted mantle lherzolite, which demonstrate residues after 12 percent partial melting of the MORB-type melt; (2) a more depleted mantle lherzolite, which asserts residues after 20 percent partial melting of the MORB-type melt. Both sources (lherzolite) were selected because these do not have significant enrichment in subduction components [25].Thus, the pillow lavas fall mainly in the MORB and BABB fields (Fig. 8c) in the Cr versus Y diagram. As it indicates they formed as a result of approximately 15-25% partial melting of plagioclase lherzolite and that they are located along the fractional crystallization trend that is controlled by removal of clinopyroxene, spinel, and olivine. However, the scheme in Figure 8c was not suitable for calculating the section of subduction

Table 3. Chemical compositions of the Arangue complex pillow lavas.

Sample	A-12	A-13	A-14	A-415	A-417	A-428	A-414	A-412	A-414	A-427
Symbol	■	■	■	■	■	■	■	■	■	■
SiO_2	40.00	44.10	40.70	43.80	41.30	40.90	42.00	42.30	44.30	47.40
TiO_2	1.60	2.00	2.00	1.70	1.60	2.10	1.80	1.60	1.80	2.30
Na_2O	2.70	4.00	3.20	3.30	3.00	2.70	2.70	2.80	3.20	4.20
MgO	5.10	4.20	5.00	6.70	6.50	4.50	5.50	5.20	6.50	5.50
Al_2O_3	13.40	13.30	14.80	14.00	14.40	13.50	14.10	14.60	15.50	14.00
P_2O_5	0.20	0.30	0.30	0.20	0.20	0.30	0.30	0.20	0.30	0.30
SO_3	0.10	<.1	0.10	<.1	0.10	0.10	<.1	0.10	0.10	0.10
K_2O	0.80	0.50	0.30	0.50	0.40	0.50	1.00	0.70	0.80	0.70
CaO	16.60	10.70	17.40	11.60	13.50	14.60	12.40	13.60	9.50	10.40
FeO	12.60	15.60	9.20	12.80	12.30	14.80	13.40	12.70	12.50	11.10
SrO	<.1	0.20	<.1	0.10	0.10	0.30	0.10	0.10	0.20	0.20
ZrO_2	<.1	0.10	<.1	<.1	<.1	0.10	<.1	<.1	0.10	0.10
Cr_2O_3	<.1	0.60	<.1	<.1	<.1	<.1	<.1	<.1	-	<.1
MnO	<.1	0.20	<.1	<.1	<.1	0.30	0.20	0.20	0.20	0.40
Total	99.70	99.50	99.20	98.70	99.40	99.20	99.90	98.70	99.90	100.20
L.O.I	6.80	3.80	6.20	4.00	6.00	4.70	6.40	4.50	4.90	3.60
Ag	<0.5	<0.5	<0.5	<0.5	<0.5	1.10	<0.5	<0.5	0.60	0.50
As	<2	<2	<2	<2	<2	2.10	<2	<2	2.40	3.70
B	160.00	150.00	273.00	163.00	237.00	161.00	229.00	211.00	126.00	144.00
Ba	104.00	78.00	78.00	55.00	69.00	83.00	98.00	174.00	160.00	99.00
Be	0.30	0.40	0.40	0.30	0.40	0.40	0.40	0.30	0.40	0.30
Bi	<1	<1	1.80	1.20	<1	<1	2.20	1.30	<1	<1
Cd	0.70	0.50	0.70	0.20	0.60	0.70	0.40	0.60	0.90	0.60
Ce	19.17	18.47	12.40	17.20	16.30	15.10	16.70	18.00	15.70	14.00
Co	34.40	38.50	35.60	33.10	42.80	31.20	38.50	31.50	34.10	41.80
Cr	310.00	313.00	433.00	485.00	449.00	304.00	391.00	320.00	232.00	265.00
Cu	27.50	38.10	29.20	19.30	23.20	36.60	16.40	30.30	40.20	78.40
Dy	4.50	4.60	4.80	4.40	4.70	4.70	4.60	4.50	4.80	4.70
Er	2.40	2.10	2.80	2.30	2.60	2.40	2.50	2.40	2.60	2.70
Eu	1.80	1.40	1.60	1.80	1.70	1.70	1.90	1.70	1.60	1.60
Ga	18.80	21.00	21.50	22.20	22.30	22.70	19.70	19.70	19.00	20.20
Gd	4.40	4.40	4.50	4.30	4.90	4.30	4.80	4.40	4.20	4.80
Ge	2.30	3.10	2.50	1.70	2.40	2.40	2.20	2.80	2.20	3.00
Hg	<1	<1	<1	<1	<1	<1	<1	<1	<1	<1
Ho	0.90	0.80	0.90	0.90	0.90	0.90	0.90	0.90	0.90	0.90
La	2.60	3.80	4.40	4.40	3.90	3.80	3.50	3.50	4.70	4.80
Li	26.00	10.80	21.00	42.50	42.30	24.50	40.90	29.40	47.10	16.20
Lu	0.40	0.60	0.40	0.40	0.40	0.50	0.40	0.50	0.40	0.60
Mn	1028.00	1393.00	1242.00	911.00	1113.00	1398.00	970.00	988.00	1316.00	2003.00
Mo	<0.5	0.80	0.70	0.60	<0.5	0.70	0.50	0.60	0.60	<0.5
Nb	1.20	4.40	2.10	2.65	2.10	4.70	3.40	2.70	2.20	3.90
Nd	15.50	16.20	15.30	16.30	15.50	15.90	16.60	15.70	16.40	16.60
Ni	98.40	79.00	118.80	87.00	105.20	56.60	93.50	70.20	95.90	110.00
P	926.00	1281.00	1053.00	819.00	907.00	991.00	932.00	793.00	1008.00	885.00
Pb	1.20	2.20	2.20	1.20	2.70	1.70	2.20	1.20	3.80	2.90
Pr	3.30	3.20	2.90	3.80	3.60	3.80	3.50	3.40	3.50	3.50
Rb	17.90	13.40	8.60	7.20	<3	11.70	9.40	10.10	15.90	15.90
S	113.00	139.20	128.30	112.60	174.30	208.30	111.30	126.20	261.20	76.00
Sb	4.10	3.20	6.10	<1	3.80	5.20	2.40	1.00	3.50	7.50
Sc	36.20	38.50	31.30	34.20	36.10	36.50	35.00	34.50	35.30	40.00
Sm	4.20	5.30	4.10	4.40	4.20	5.20	4.30	4.90	4.50	5.30
Sn	5.10	5.90	4.90	4.30	4.60	5.60	4.80	4.90	4.90	6.40
Sr	239.00	919.00	165.00	363.00	267.00	1505.00	447.00	734.00	1175.00	1591.00
Ta	3.60	3.50	3.40	2.70	2.40	3.20	3.70	2.50	2.90	5.00
Tb	0.80	0.80	0.80	0.80	0.90	0.80	0.80	0.90	0.90	0.90
Te	0.80	1.00	0.80	0.80	0.70	0.90	0.80	0.80	0.70	1.10
Th	0.17	0.19	0.19	0.15	0.19	0.13	0.19	0.19	0.13	0.11

components to mantle lherzolite. Consequently, the diagram in Figure 8d was used to estimate the share of subduction components. High ratio Ba/Th proposes that the mantle source of the pillow lavas in Arangue complex were mainly affected by the addition of aqueous fluids (Fig. 8d). This geodynamic environment is schematically shown in Figure 9. A likely model may assert the formation of the pillow lava from the Arangue

Table 3. Ctd

Sample	A-12	A-13	A-14	A-415	A-417	A-428	A-414	A-412	A-414	A-427
Symbol										
Tl	1.10	1.60	0.80	1.40	1.60	1.10	1.30	0.60	0.80	0.50
Tm	0.30	0.32	0.40	0.40	0.40	0.30	0.30	0.30	0.30	0.30
Ti	8401.00	10215.00	8998.00	8545.00	8726.00	9797.00	8826.00	8284.00	9062.00	>10000
U	0.50	0.50	0.20	0.50	0.20	0.90	0.90	0.40	0.10	0.70
V	236.00	251.00	222.00	230.00	231.00	237.00	240.00	234.00	259.00	213.00
Y	22.10	20.20	24.70	21.30	23.30	26.80	21.80	21.40	22.40	22.60
Yb	2.40	2.70	2.40	2.70	2.30	2.60	2.10	2.10	2.10	2.40
Zn	62.70	85.00	60.50	33.00	60.60	17.80	32.10	28.50	221.20	98.80
Zr	103.90	104.50	132.90	119.80	123.90	184.20	144.30	107.30	139.90	117.70
Nb/Y	0.05	0.22	0.09	0.12	0.09	0.18	0.16	0.13	0.10	0.17
Zr/Y	4.70	5.17	5.38	5.62	5.32	6.87	6.62	5.01	6.25	5.21
Th/Ta	0.05	0.05	0.06	0.06	0.08	0.04	0.05	0.08	0.04	0.02
La/Nb	2.17	0.86	2.10	1.66	1.86	0.81	1.03	1.30	2.14	1.23
Eu/Eu*	1.28	0.89	1.14	1.27	1.15	1.10	1.28	1.12	1.13	0.97
Ba/Th	611.76	410.53	410.53	366.67	363.16	638.46	515.79	915.79	1230.77	900.00
Th/Nb	0.14	0.04	0.09	0.06	0.09	0.03	0.06	0.07	0.06	0.03

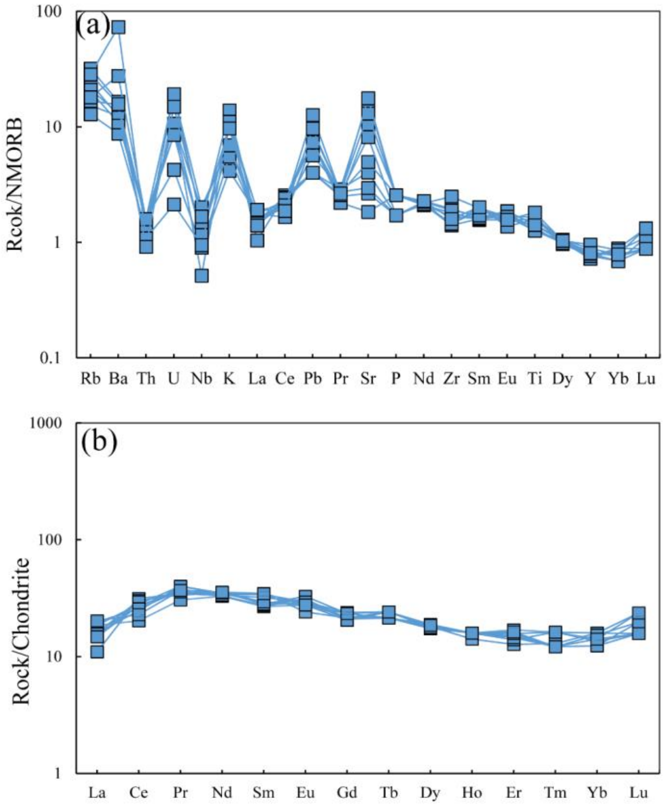

Figure 7. (a) N- MORB normalized spider diagram for the Arangue complex. (Normalization values are from [43]). (b) Chondrite-normalized diagram for the Arangue complex. Normalization values are from [43]. Symbols are the same as in Table 3.

Complex.

Conclusion

The Arangue complex in the southeast of the city of Hormozgan, belongs to the Makran structural zone. This complex consists of ultra-mafic rocks, microgabbro dykes, pillow lavas and lime stones that pillow lavas are mainly exposed to the northwest and southeast part of study area. Based on mineral geochemistry, plagioclases and clinopyroxene composition varies from $An_{68.27-81.73}$ $Ab_{18.27-31.57}$ $Or_{0-0.41}$ and $Wo_{38.1-47.8}Fs_{8.2-19.3}$ $En_{38.6-48.7}$ respectively. Geochemical data indicate that the

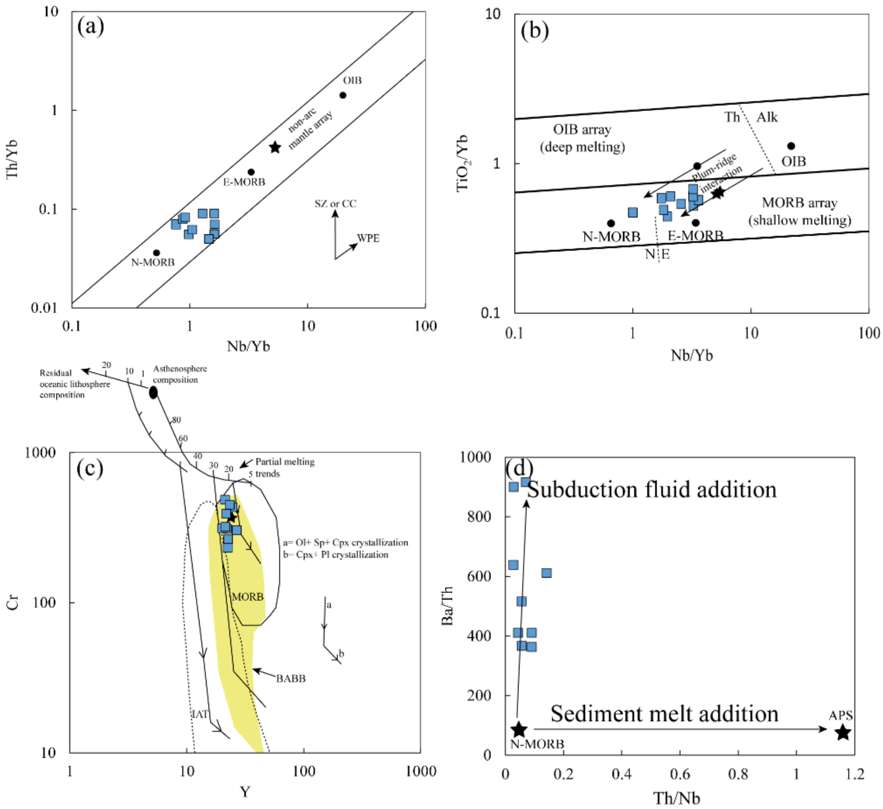

Figure 8. (a) Plot of Th/Yb versus Nb/Yb [45] for the Arangue complex pillow lavas [43]. (b) TiO_2/Yb versus Nb/Yb diagram [46] of the Arangue complex pillow lavas [43]. (c) Cr-Y diagram [42] for the Arangue complex pillow lavas. (d) Ba/Th versus Th/ Nb diagram for Arangue complex pillow lavas. Star show the average composition of politic sediments (APS, [47]) and N-MORB, [43]. Symbols are the same as in Table 3.

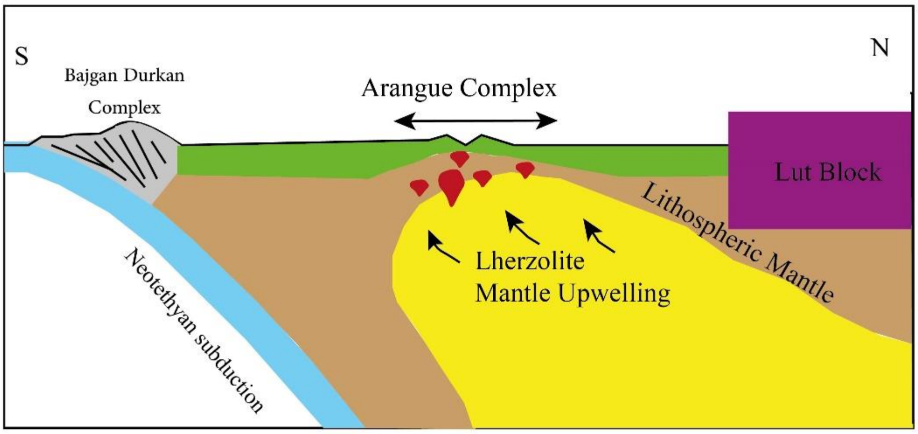

Figure 9. Schematic drawing showing a possible tectonic model for the generation of Arangue ophiolitic complex that eventually led into the formation of pillow lava flows.

Arangue complex pillow lavas are tholeiitic and show properties similar to transitional basalts between enriched MORB and OIB and some BABB. However, their enrichment in incompatible elements and low Nb and La / Nb ratios (0.8-2.1) display that these have affinity of the BABB. These were likely produced by nearly 15-25% partial melting of mantle lherzolite. Ba / Th versus Th / Nb diagrams show that the source of mantle lherzolite is subjected to enrichment variables in subduction derived components consisting of fluids for the Arangue Complex pillow lavas.

Acknowledgements

We would like to thank the University of Hormozgan for their financial supports.

References

1. Dilek Y, Furnes H. Ophiolite genesis and global tectonics: Geochemical and tectonic fingerprinting of ancient oceanic lithosphere. Bulletin. 2011; 123(3-4): 387-411.
2. Moghadam HS, Corfu F, Chiaradia M, Stern RJ, Ghorbani G. Sabzevar Ophiolite, NE Iran: Progress from embryonic oceanic lithosphere into magmatic arc constrained by new isotopic and geochemical data. Lithos. 2014; 210: 224-241.
3. Saccani E, Delavari M, Beccaluva L, Amini S. Petrological and geochemical constraints on the origin of the Nehbandan ophiolitic complex (eastern Iran): Implication for the evolution of the Sistan Ocean. Lithos. 2010; 117(1-4):209-228.
4. Arvin M, Robinson PT. The petrogenesis and tectonic setting of lavas from the Baft ophiolitic mélange, southwest of Kerman, Iran. Can. J. Earth. Sci. 1994; 31(5):824-834.
5. Shahzeidi M, Moayyed M, Murata M, Yui TF, Arai S, Chen F, Pirnia T, Ahmadian J. Late Ediacaran crustal thickening in Iran: Geochemical and isotopic constraints from the~ 550 Ma Mishu granitoids (northwest Iran). Int. Geol. Rev. 2017; 59(7):793-811.
6. Torabi Gh. Metamorphism of mantle peridotites in Jandaq ophiolite (Central Iran). J. Petrol (In Persian). 2012; 3 (11): 1-18.
7. Baluchi S, Sadeghian M, Ghasemi H, Mingo J, Lee CL, Yanbin J. Mineral chemistry, geochronology and isotopic geochemistry of Rb-Sr and Sm-Nd Iraqi granites. Kharazmi. J. Earth Sci (In Persian). 2017; 3 (2): 160-139.
8. Haghipour A. Precambrian in central Iran: lithostratigraphy, structural history and petrology. Iran. Petroleum. Institute. Bullet. 1981; 81: 1–17.
9. Hajialioghli R, Moazzen M, Droop G T R, Oberhansli R, Bousquet R, Jahangiri A, Ziemann M. Serpentine polymorphs and P-T evolution of meta-peridotites and serpentinites in the Takab area, NW Iran. Mineral. Mag. 2007; 71: 155–174.
10. Saki A. Proto–Tethyan remnants in northwest Iran: Geochemistry of the gneisses and metapelitic rocks. Gondwana. Res. 2010; 17(4): 704–714.
11. Khalatbari-Jafari M, Juteau T, Bellon H, Emami H. Discovery of two ophiolite complexes of different ages in the Khoy area (NW Iran). Comptes. Rendus. Geoscience. 2003; 335 (12): 917-929.
12. Khalatbari-Jafari M, Juteau T, Bellon H, Whitechurch H, Cotten J, Emami H. New geological, geochronological and geochemical investigations on the Khoy ophiolites and related formations, NW Iran. J. Asian. Earth. Sci. 2004; 23 (4): 507-535.
13. Khalatbari-Jafari M, Juteau T, Cotten J. Petrological and geochemical study of the Late Cretaceous ophiolite of Khoy (NW Iran), and related geological formations. J. Asian. Earth. Sci. 2006; 27(4): 465-502.
14. Stöcklin J. Northern iran: Alborz Mountains. Geological Society, London, Special Publications. 1974; 4(1):213-234.
15. Sahandi MR, Soheili M. 1/100000 Geological map of Iran. Geology Survey and Mineral Exploration of Iran. 2014; 5: 214-215.
16. Pirouz M, Avouac JP, Gualandi A, Hassanzadeh J, Sternai P. Flexural bending of the Zagros foreland basin. Geophysic. J. Int. 2017; 210(3):1659-1680.
17. Moghadam HS, Stern RJ. Ophiolites of Iran: Keys to understanding the tectonic evolution of SW Asia :(II) Mesozoic ophiolites. J. Asian. Earth. Sci. 2015; 100:31-59.
18. Samimi Namin M. 1/250000Taheruiyeh geological map. Geology Survey and Mineral Exploration of Iran. 1982; 2: 113-114.
19. McCall GJ, Kidd RG. The Makran, Southeastern Iran: the anatomy of a convergent plate margin active from Cretaceous to Present. Geological Society, London, Special Publications. 1982; 10(1):387-397.
20. Ghazi AM, Hassanipak AA, Mahoney JJ, Duncan RA. Geochemical characteristics, 40Ar–39Ar ages and original tectonic setting of the Band-e-Zeyarat/Dar Anar ophiolite, Makran accretionary prism, SE Iran. Tectonophysics. 2004; 393(1-4):175-196.
21. Moslempour ME, Khalatbari-Jafari M, Morishita T, Ghaderi M. Petrology and Geochemistry of Peridotites fromFannuj-Maskutan Ophiolitic Complex, Makran Zone, SE Iran. J. Geosci. 2013; 22(87):181-196.
22. Moslempour ME, Khalatbari-Jafari M, Ghaderi M, Yousefi H, Shahdadi S. Petrology, geochemistry and tectonics of the extrusive sequence of Fannuj-Maskutan ophiolite, Southeastern Iran. J. Geol. Soc. India. 2015; 85(5):604-618.
23. Sepidbar F, Lucci F, Biabangard H, Zaki Khedr M, Jiantang P. Geochemistry and tectonic significance of the Fannuj-Maskutan SSZ-type ophiolite (Inner Makran, SE Iran). Int. Geol. Rev. 2020; 62(16):2077-2104.
24. Shahabpour J. Tectonic implications of the geochemical data from the Makran igneous rocks in Iran. Island Arc. 2010; 19: 676-689.
25. Saccani E, Delavari M, Dolati A, Marroni M, Pandolfi L, Chiari M, Barbero E. New insights into the geodynamics of Neo-Tethys in the Makran area: Evidence from age and petrology of ophiolites from the Coloured Melange Complex (SE Iran). Gondwana. Res. 2017; 62: 306-327.
26. Siddiqui RH, Jan MQ, Khan MA. Petrogenesis of late Cretaceous lava flows from a Ceno-Tethyan island arc: The Raskoh arc, Balochistan, Pakistan. J. Asian. Earth. Sci. 2012; 59:24-38.
27. Burg JP, Dolati A, Bermoulli D, Smit J. Structural style of the Makran tertiary accretionary complex in SE-Iran, in Al, H.K., Roure F., Ellison R., and Lokier S., eds., Lithosphere dynamics and sedimentary basins: The Arabian Plate and analogues Front. Earth Sci. 2013; 2: 239-259.

28.Walker GP. Morphometric study of pillow-size spectrum among pillow lavas. Bullet. Volcanol. 1992; 54(6):459-474.
29.Sinton J, Bergmanis E, Rubin K, Batiza R, Gregg TK, Grönvold K, Macdonald KC, White SM. Volcanic eruptions on mid-ocean ridges: New evidence from the superfast spreading East Pacific Rise, 17–19 S. J. Geophysic. Res: Solid Earth. 2002; 107(B6): ECV-3.
30.Whitney DL, Evans BW. Abbreviations for names of rock-forming minerals. Am. Mineral. 2010; 95(1):185-187.
31.Deer WA, Howie RA, Zussman J. An introduction to the Rock-Forming Minerals: Longman, London. 1992; 1:1-696.
32.Morimoto N, Fabries J, Ferguson AK, Ginzburg IV, Ross M, Seifert FA, Zussman J, Aoki K, Gottardi G. Nomenclature of pyroxenes. Mineral. Mag. 1988; 52: 535-550.
33.Pearce JA, Norry MJ. Petrogenetic implications of Ti, Zr, Y, and Nb variations in volcanic rocks. Contribut. Mineral. Petrol. 1979; 69(1):33-47.
34.Venturelli G, Thorpe RS, Potts PJ. Rare earth and trace element characteristics of ophiolitic metabasalts from the Alpine-Apennine belt. Earth. Planet. Sci. Lett. 1981; 53(1):109-123.
35.Humphris SE, Thompson G. Trace element mobility during hydrothermal alteration of oceanic basalts. Geochim. Cosmochim. Acta. 1978; 42(1):127-36.
36.Daly K.B. A study of the mafic plutons along the Bloody Bluff Fault in northeastern Massachusetts: Placing constraints on the tectonic environment using geochemical and petrologic analysis. M.Sc. thesis, Boston College. 2003; 1-157p.
37.Shervais JW. Ti-V plots and the petrogenesis of modern and ophiolitic lavas. Earth. Planet. Sci. Lett. 1982; 59(1):101-118.
38.Wang Z, Wilde SA, Wang K, Yu L. A MORB-arc basalt–adakite association in the 2.5 Ga Wutai greenstone belt: late Archean magmatism and crustal growth in the North China Craton. Precambrian. Res. 2004; 131(3-4):323-343.
39.Yuan C, Sun M, Zhou MF, Xiao W, Zhou H. Geochemistry and petrogenesis of the Yishak Volcanic Sequence, Kudi ophiolite, West Kunlun (NW China): implications for the magmatic evolution in a subduction zone environment. Contribut. Mineral. Petrol. 2005; 150(2):195-211.
40.Winchester JA, Floyd PA. Geochemical discrimination of different magma series and their differentiation products using immobile elements. Chem. Geol. 1977; 20:325-43.
41.Saunders AD, Tarney J. The geochemistry of basalts from a back-arc spreading centre in the East Scotia Sea. Geochim. Cosmochim. Acta. 1979; 43(4):555-72.
42.Pearce JA, Alabaster T, Shelton AW, Searle MP. The Oman ophiolite as a Cretaceous arc-basin complex: evidence and implications. Philosophical Transactions of the Royal Society of London. Series A, Math. Physic. Sci. 1981; 300(1454):299-317.
43.Sun SS, McDonough WF. Chemical and isotopic systematics of oceanic basalts: implications for mantle composition and processes. Geological Society, London, Special Publications. 1989; 42(1):313-45.
44.Pearce JA. Role of the sub-continental lithosphere in magma genesis at active continental margin. In: Hawkesworth CJ, Norry MJ, (Eds.), continental basalts and mantle xenoliths. Shiva Publishing, Cheshire, United Kingdom. 1983; 24: 230-249.
45.Pearce JA, Peate DW. Tectonic implications of the composition of volcanic arc magmas. Annu. Rev. Earth. Planet. Sci. 1995; 23:251-286.
46.Pearce JA. Geochemical fingerprinting of oceanic basalts with applications to ophiolite classification and the search for Archean oceanic crust. Lithos. 2008; 100: 14-48.
47.Taylor SR, McLennan SM. The continental crust: its composition and Evolution; an Examination of the Geochemical Record Preserved in Sedimentary Rocks. Blackwell Scientific Publication, Oxford. 1985; 1: 1-312.
48.Murton BJ. Tectonic controls on boninite genesis. Geological Society, London, Special Publications. 1989; 42(1):347-377.